

Pulsed discharge nozzle cavity ringdown spectroscopy of cold polycyclic aromatic hydrocarbon ions

Ludovic Biennier,^{a)} Farid Salama, and Louis J. Allamandola
NASA-Ames Research Center, Space Science Division, MS 245-6, Moffett Field, California 94035-1000

James J. Scherer^{b)}
Los Gatos Research, Mountain View, California 94041

(Received 27 September 2002; accepted 6 February 2003)

The gas-phase electronic absorption spectra of the naphthalene ($C_{10}H_8^+$) and acenaphthene ($C_{12}H_{10}^+$) cations have been measured in the visible range in a free jet planar expansion in an attempt to collect data in an astrophysically relevant environment. The direct absorption spectra of two out of four bands measured of the gas-phase cold naphthalene cation along with the gas-phase vibronic absorption spectrum of the cold acenaphthene cation are reported for the first time. Direct absorption spectra of their van der Waals complexes with argon are also reported for the first time. The study has been carried out using the ultrasensitive and versatile technique of cavity ringdown spectroscopy (CRDS) coupled to a pulsed discharge slit nozzle (PDN). The new PDN-CRDS set up is described and its characteristics are evaluated. The direct-absorption spectra of the polycyclic aromatic hydrocarbon (PAH) ions are discussed and compared to the gas-phase and solid-phase data available in the literature. The analysis of the results show that cold, free flying PAH ions are generated in the argon discharge primarily through soft Penning ionization. This enables the intrinsic band profiles to be measured, a key requirement for astrophysical applications. © 2003 American Institute of Physics. [DOI: 10.1063/1.1564044]

I. INTRODUCTION

Polycyclic aromatic hydrocarbons (PAHs) play an important role in astrophysics and have been the target of extensive laboratory studies (for a recent review, see Ref. 1). PAHs are found in meteorites and interplanetary dust particles and have been suggested to carry the ubiquitous unidentified infrared bands seen in emission in a wide variety of interstellar and extragalactic environments² as well as some of the 300 diffuse interstellar bands (DIBs) seen in absorption in the spectra of diffuse interstellar clouds.^{3,4} The identification of the DIBs is the longest standing problem in astrophysical spectroscopy (for a review see Ref. 5). The present consensus is that the DIBs arise from *gas-phase* organic molecules and/or ions that are abundant under the typical conditions reigning in the diffuse interstellar medium (ISM).^{6,7} A significant fraction of PAHs is expected to be ionized in the diffuse ISM.⁸ In order to unambiguously assess the validity of the PAH proposal, it is essential to measure the electronic absorption spectra of neutral and ionized PAHs under conditions that come close to the conditions found in the interstellar medium, i.e., free, cold, molecules and ions. Until very recently, laboratory measurements relied on matrix isolation spectroscopy (MIS) where PAHs are isolated in a solid rare gas matrix at very low temperature and submitted to vacuum ultraviolet radiation to mimic the ISM conditions.¹ However, even in the least perturbing (low polarizability) neon matrices the interaction of the trapped PAHs with the rare gas atoms of the solid lattice induces a frequency shift and a broadening of the band profile that

preclude a decisive comparison with astronomical data. MIS surveys over a broad spectral range are critical however for the pre-selection of the most promising candidates.¹

Measuring the spectra of PAH ions in the gas phase represents an experimental challenge because PAHs are large, nonvolatile molecules that need to be vaporized and ionized. Furthermore, due to the ultrafast nonradiative processes of internal electronic conversion that take place in these large molecular systems, detection by laser-induced fluorescence or by multiphoton excitation cannot be employed. The molecular spectroscopy of PAH ions in the gas phase has thus remained unexplored until only very recently when two groups succeeded in measuring the electronic absorption spectra of cold PAH ions in the gas phase.^{9,10}

We report, here, direct absorption measurements in the gas phase of electronic bands of the naphthalene and the acenaphthene cations and describe the cavity ringdown spectrometer-pulsed discharge nozzle (PDN-CRDS) system that has been developed at NASA-Ames to measure the gas phase spectra of neutral and ionized interstellar PAH analogs. The CRD spectrometer and the cold plasma source are described in Sec. II. Section III presents and discusses the gas-phase absorption spectra of the cold naphthalene and acenaphthene ions. The conclusions are discussed in Sec. IV.

II. EXPERIMENT

A schematic of the experimental setup is shown in Fig. 1. The apparatus consists of a pulsed discharge slit nozzle (PDN) mounted in a vacuum chamber and coupled to a high-finesse optical cavity. The plasma expansion generated by the PDN is probed by a cavity ringdown spectrometer several mm downstream with a sub-ppm to ppm sensitivity. The

^{a)}Electronic mail: lbiennier@mail.arc.nasa.gov

^{b)}Current address: Novawave Technologies, Redwood Shores, California.

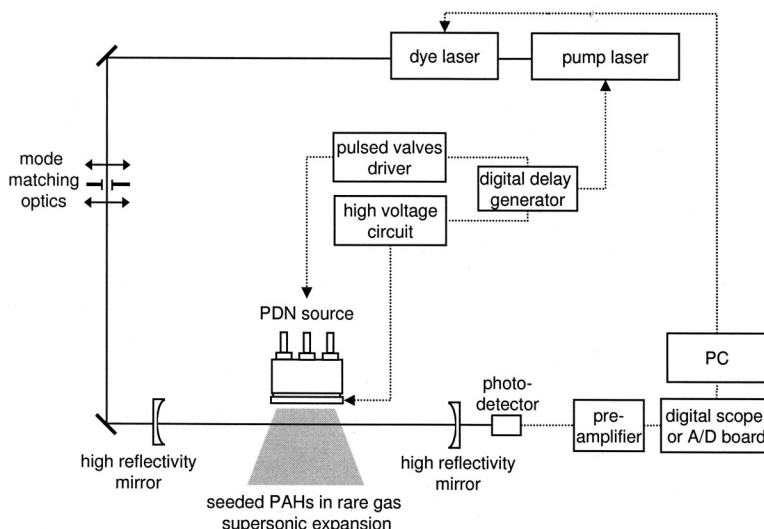


FIG. 1. Schematic of the pulsed-discharge-nozzle cavity ringdown spectrometer (PDN-CRDS) experimental apparatus (see the text for details and Fig. 3 for the timing sequence).

spectrometer is based on a pulsed dye laser for the injection of visible photons into the high-finesse cavity. A photodetector, connected to a high-speed scope or A/D board, is used for the detection of the visible photons leaking out of the rear mirror of the cavity. Individual components are described in detail in the following.

A. The cold plasma source: pulsed discharge nozzle

The PDN combines a supersonic slit free jet with two electrodes that produce a discharge in the stream of the planar expansion.¹¹ The pulsed supersonic slit jet is based on a design by Saykally and co-workers.¹² The source body consists of a heated copper reservoir onto which three synchronized pulsed solenoid valves (General Valve Series 9) have been adapted to drive the retraction of a 10-cm-long armature that seals the slit from the inside. The slit aperture was produced using electro-machining methods ensuring a uniform gap 200 μm wide and 10 cm long. The PAH sample (Sigma Aldrich, $\geq 95\%$ purity) can be solid or liquid at room temperature and is placed in a 25 cm^3 sample reservoir mounted on the bottom of the source. The sample can be heated up to 250 $^\circ\text{C}$ to increase its vapor pressure. Two ceramic heater strips attached at the bottom and on the top of the PDN assembly provide the heating. The top of the PDN assembly is always maintained at a slightly higher temperature than the bottom part ($\Delta T \sim 2^\circ\text{C}$) to avoid condensation of the high-refractory PAHs on the internal edges of the nozzle. A typical argon gas pulse (99.985% purity) of 1 atm backing pressure and lasting 1.2 ms generates a background pressure of 150 mTorr in the expansion chamber at 10 Hz.

Two polished stainless steel knife-edge electrode jaws are mounted on each side of the slit. The two electrodes are insulated from the PDN assembly by a 1.5-mm-thick Macor rectangular plate possessing a slit opening equal to twice the width of the nozzle (400 μm). An even gap (typically 400 μm) is maintained between the jaws. Figure 2 gives the schematic of the high voltage pulse generator.¹³ It is based on (i) a low current HV source (-1200 V , 75 mA) and a 10 k Ω

resistor limiting the input current, (ii) a high capacitor (45 μF) maintaining a constant voltage when discharging, (iii) a fast switching n -channel field effect transistor (MTP3N120E) that is capable of operating at high voltages, (iv) a commercial radio transformer controlling the gate of the transistor and isolating the HV circuit from (v) the pulse control generator (+10 V), and (vi) two independent ballast lines (1 k Ω). A negative voltage pulse (-400 to -600 V) is independently applied to both electrodes through the two separate 1 k Ω ballast resistors while the source body is independently grounded via a small 50 Ω resistor to provide a current return path and a way to measure it. This implementation ionizes the seeded carrier gas pulse directly in the stream of the jet. The amplitude of the current ($\sim 50\text{ mA}$) can also be derived from the measurement of the jaw voltage as illustrated in the bottom trace of Fig. 3. The transient decrease in the magnitude of the jaw voltage is a measure of the voltage drop across the ballast resistor, which is in turn a

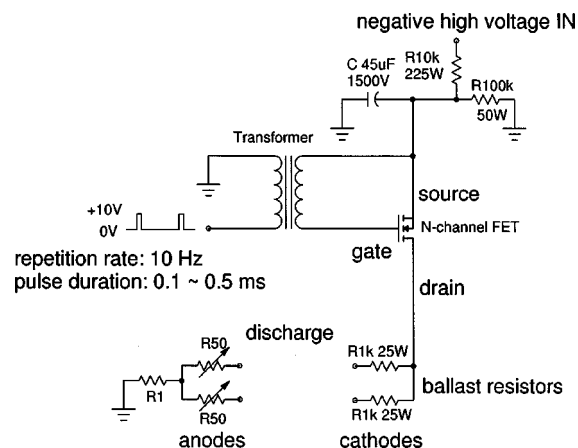


FIG. 2. High voltage electrical circuit. Adapted from Ref. 13. Typical operational conditions are -500 V for the applied voltage and 50 mA for the measured current.

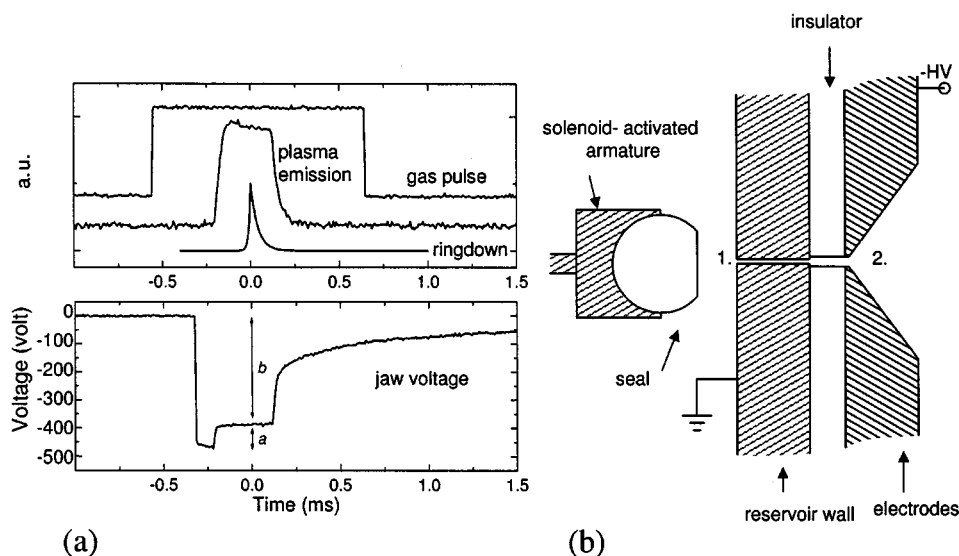


FIG. 3. (a) Time sequence. The time sequence is empirically optimized. Typical operational conditions are as follows: The gas pulse duration is ~ 1000 – $1200 \mu\text{s}$, the HV discharge is applied for $\sim 500 \mu\text{s}$, the ringdown is $\geq 100 \mu\text{s}$ and starts midway through the gas pulse duration. The arrow *a* is the measure of the discharge current flowing through the ballast resistors and arrow *b* is the measure of the discharge voltage. (b) Cross section of the PDN source. 1. $200 \mu\text{m} \times 10 \text{ cm}$ slit. 2. $400 \mu\text{m}$ cathode gap.

direct measure of the instantaneous current through the discharge.

The plasma is expanded in a 25 cm cubic stainless steel chamber equipped with four ports. One port is used to mount the PDN assembly. A transparent window is mounted on the opposite port for visual observation of the jet expansion. The two remaining ports are equipped with two 2.5-cm-diam, 15-cm-long, cylindrical arms designed to accommodate vacuum-compatible mirror mounts (Los Gatos Research). The chamber is extended in order to reduce the formation of a deposit on the optical surfaces of the ringdown cavity. Further isolation is provided by inserting baffles into the arms of the cavity and by circulating a continuous flow of argon in front of the mirrors. The gas expansion is evacuated perpendicularly to the expansion plane by a mechanical booster pump (Edwards, EH-1200) that is backed by a dry pump (Edwards, GV-250). The pumping capacity of the system is 250 l/s. The jet assembly can be moved back and forth and up and down from the outside to probe the planar expansion from 0 to 2 cm downstream, although the expansion is usually probed in the postdischarge region (2 mm downstream the electrode jaws) where the absorption signal is maximum.

B. Cavity ringdown spectrometer

Cavity ringdown spectroscopy is based on the measurement of the lifetime of photons trapped in a stable high-finesse optical cavity formed by two high-reflectivity concave mirrors.¹⁴ Photons are injected into the cavity through the front mirror when the laser spectral linewidth overlaps with at least one cavity mode. A photodetector is used to monitor the exponential decay of the number of photons escaping the cavity through the rear mirror, with a characteristic time that depends on the intrinsic losses of the cavity (transmission, scattering, and absorption by the mirrors) and losses due to the gaseous absorbent present in the cavity. In the high reflectivity mirror limit, the decay rate can be written as

$$\frac{1}{\tau} = \frac{T + \mathcal{L} + \alpha l}{l/c} = \frac{1}{\tau_0} + c\alpha \quad (1)$$

with T , the transmittivity, \mathcal{L} , the small losses due to the direct absorption by the multilayer dielectric coating and the scattering from the surface irregularities, α , the absorption coefficient of the gaseous sample present in the cavity, l , the cavity length, c , the speed of light, and τ_0 , the photon confinement time of the empty cavity. Once the decay rate for a fixed wavelength has been determined, the laser is tuned and the procedure repeated to acquire a whole spectrum corresponding to the sum of the intrinsic losses, which vary slowly with the frequency over the broad reflectivity curve of the mirror, and the absorption due to the gaseous species contained in the cavity. The same procedure is repeated with the empty cavity. The absolute absorbance associated with the sample is determined by subtracting the baseline losses from those obtained with the PDN source functioning. In the case of PAH ions, the sample absorption bandwidth is broader than the laser linewidth and the measurements remain quantitative. Their spectra are not affected by nonlinear absorption effects due to the injection in the cavity of modes encountering nonhomogeneous losses that would, otherwise, result in the underestimation of the concentration.

The laser source of the NASA–Ames CRD spectrometer is a 0.1 cm^{-1} linewidth, tunable, pulsed Continuum ND6000 dye laser that is pumped by the second harmonic of a Nd:YAG Quanta Ray DCR 1A, operating at 10 Hz. The excitation of pure longitudinal cavity modes that is essential for the conservation of the monoexponential behavior of the trapped photon decay is aided by mode matching the incident laser pulse using two lenses and a pinhole (50 – $80 \mu\text{m}$ diameter). This optical configuration also helps spatially filter the incoming non-Gaussian beam. The ringdown cavity is composed of two concave dielectric super mirrors (Los Gatos Research), 99.99%–99.999% reflectivity coefficient, 6 m curvature radius, mounted $l = 55 \text{ cm}$ apart. The high reflectivity curve of the mirrors covers typically $\sim 12\%$ of the wavelength of maximum reflection i.e., 70 nm at 600 nm. The beam waist remains almost constant ($\geq 500 \mu\text{m}$ diameter) along the 10 cm probing column. A photomultiplier tube (Hamamatsu R955) is used to detect the ringdown pho-

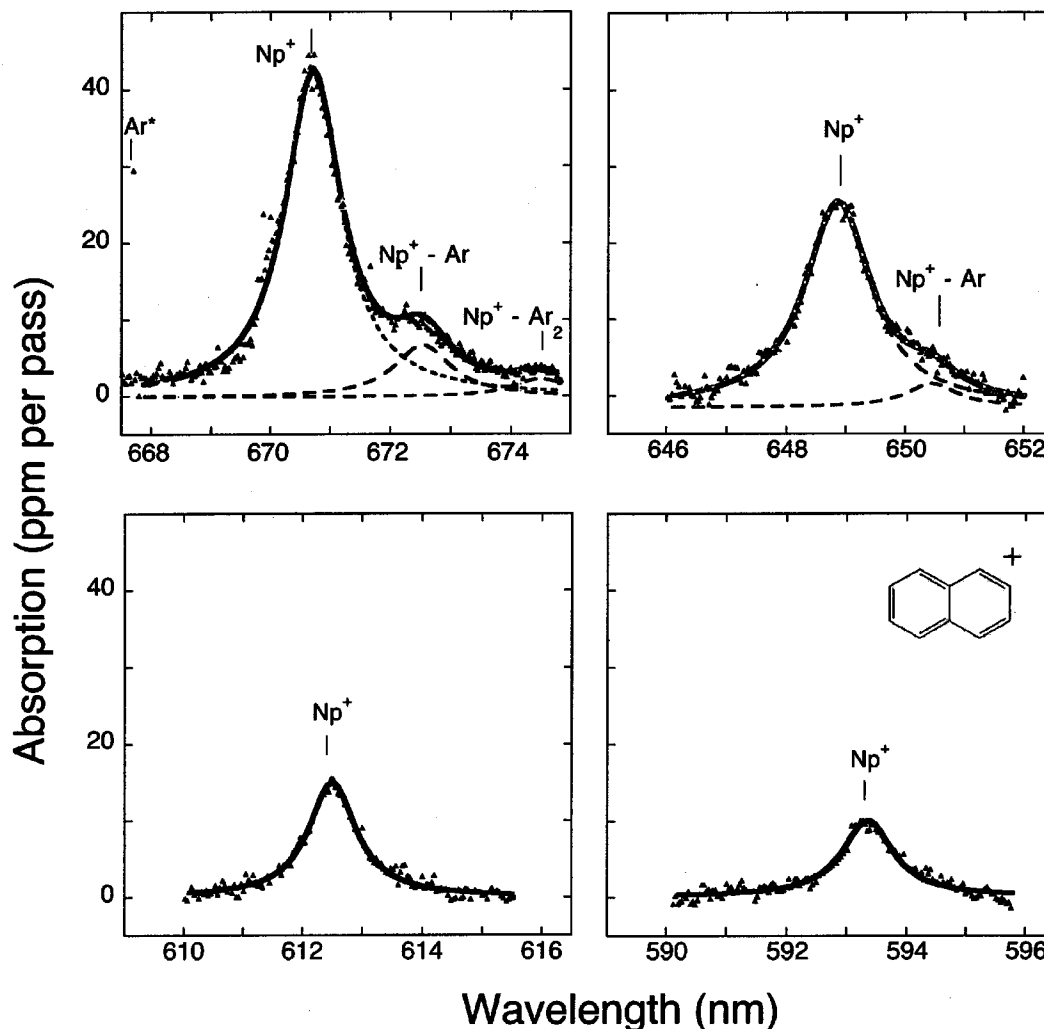


FIG. 4. Gas phase absorption spectrum of the four stronger vibronic bands of the $D_2 \leftarrow D_0$ electronic transition band system of Np^+ . The vibronic bands were all measured individually in separate spectral windows.

tons that leak out of the cavity. A narrowband filter is used to dramatically reduce the stray photons arising from the characteristic glow emission of the carrier gas (Ar or Ne) plasma. The photocurrent is subsequently amplified by a *trans*-impedance circuit and digitized by a 500 MHz 9 bit oscilloscope (Textronix TDS 3052) or a 20 MHz 12 bit digital acquisition board (Adlink, PCI9812-2). The data are then processed in a PC by a LABVIEW program that has been developed to carry out treatment of the digital signal and

extraction of the cavity losses. Each ringdown event is triggered on its falling slope at a given threshold and fitted independently with an exponential decay wave form with a floating baseline determined by sampling 10 data points before the trigger. The ringdown time of the 55 cm cavity lasts from 20 to 100 μs depending on the reflectivity of the dielectric mirrors. Given the 10-cm-long absorption column of the PDN, these decay times correspond to effective path lengths of 1–5 km. The noise level is better than 0.1 ppm for

TABLE I. Naphthalene ion ($\text{C}_{10}\text{H}_8^+$) absorption peak positions and widths of the vibronic bands for the $D_2 \leftarrow D_0$ electronic band system.

Assignment	Gas phase						Solid phase		
	λ^e (nm)	PDN-CRDS ^a		cw-jet CRDS ^b		Photodepletion ^c		MIS/Ne ^d	
		ν^f (cm^{-1})	$\Delta\nu$ (cm^{-1})	λ (nm)	$\Delta\nu$ (cm^{-1})	λ (nm)	$\Delta\nu$ (cm^{-1})	λ (nm)	$\Delta\nu$ (cm^{-1})
0	670.70	14905.7	25	670.65	31	670.69	23	674.1	120
$\nu_9(a_g)$	648.89	15406.7	25	648.84	43	648.93	...	652.0	...
$\nu_4(a_g)$	612.52	16321.5	27			612.48	...	615.1	...
$\nu_9(a_g) + \nu_4(a_g)$	593.35	16848.8	31			593.4	...	596.5	...

^aThis work.

^bcw-jet expansion pulsed discharge CRDS. Romanini *et al.* (Ref. 9).

^cPino *et al.* (Ref. 18).

^dSalama *et al.* (Ref. 19).

^eAir wavelength.

^fVacuum wave numbers.

the “empty” cavity and reaches 1–2 ppm loss per pass when the plasma is expanding. The increase of the noise level is primarily due to scattering by the plasma, and more marginally to the incomplete blocking of the fluctuating blue emission of excited argon atoms that superimpose with “ring-down” photons leaking out of the cavity. We usually average 8–20 laser shots before tuning the laser wavelength. The spectrum is finally processed by an 11 points ($\sim 1 \text{ cm}^{-1}$) Savitsky–Golay smoothing procedure¹⁵ that keeps the line shape distortion minimum. The wavelength calibration is performed by using the well-documented absorption line positions of metastable argon.¹⁶

The time sequence followed in the experiments is depicted in Fig. 3. It is an empirical optimization of the sequence adopted by Motylewski and Linnartz.¹⁷ A multichannel pulse generator controls a pulsed valve driver (General Valves, Iota One) for gas admission, a homemade high-voltage discharge circuit and the firing of the laser. In a typical experiment, the gas pulse duration is set to 1.0–1.2 ms and can be monitored by delaying the discharge firing. The high-voltage pulse is kept on two to three times longer than the ringdown event and starts $\sim 500 \mu\text{s}$ after the solenoid valves open. A short delay is maintained between the high voltage switch on and the triggering of the laser. Monitoring the fluorescence and/or phosphorescence of the metastable Ar atoms and ions (observed when the narrowband filter is removed) helps to optimize discharge timing.

III. RESULTS AND DISCUSSION

The visible absorption spectra of the gas-phase naphthalene ($\text{C}_{10}\text{H}_8^+$) and acenaphthene ($\text{C}_{12}\text{H}_{10}^+$) cations have been measured with the newly developed instrument. In the case of the naphthalene cation, four vibronic bands of the first electronic band system have been measured through CRDS. Two out of four bands are measured for the first time in direct absorption completing and expanding our prior cavity ringdown work.⁹ The bands were all measured individually in separate wavelength windows defined by the convolution of the response curve of the high reflectivity mirrors and the dye laser output (see Sec. II). Band relative intensities were scaled using the data available in the literature.^{9,18} The measurements are compared with detailed matrix isolation spectra¹⁹ data and with the data derived from the method of gas-phase molecular depletion.¹⁸ These comparisons bring conclusive evidence regarding the vibrational states of the probed naphthalene cations ($\text{C}_{10}\text{H}_8^+$). The electronic absorption spectrum of the acenaphthene cation ($\text{C}_{12}\text{H}_{10}^+$) is reported for the first time in the gas phase and compared to MIS data.²⁰ The presentation of the spectra is followed by the discussion of the ion formation mechanism.

A. The naphthalene ion ($\text{C}_{10}\text{H}_8^+$)

Naphthalene is a planar hydrocarbon that belongs to the D_{2h} symmetry group. We have adopted the configuration where the x and y axes correspond to the long and short axes of the molecule, respectively. The first four strong absorption bands belonging to the vibrational progression of the ${}^2B_{3g}(D_2) \leftarrow X{}^2A_u(D_0)$ electronic band system of Np^+

($\text{C}_{10}\text{H}_8^+$) have been measured and are shown in Fig. 4. Measurements were performed at a $\sim 70^\circ\text{C}$ reservoir temperature, under ~ 760 Torr backing pressure and ~ -500 V applied voltage. The 670.70 and the 648.89 nm bands are in perfect agreement with our previous CRDS measurements⁹ while the 612.52 and the 593.35 nm bands are measured for the first time through direct absorption CRDS. The four vibronic bands have been previously assigned¹⁹ by analogy with the spectrum of neutral naphthalene to transitions involving the out-of-plane distortion mode $\nu_9(a_g)$ and the C–C stretching vibration mode of the bond common to both rings $\nu_4(a_g)$ and are listed in Table I where the measured frequencies are also compared with the values obtained by MIS in a Ne matrix,¹⁹ cw-jet expansion CRDS,⁹ and photodissociation of the $\text{Np}^+ - \text{Ar}$ complex prepared by resonant two-photon two-color ionization (R2P2CI).¹⁸ The band peak positions are determined with an accuracy better than ± 0.05 nm and in excellent agreement with the measurements from previous gas-phase experiments.^{9,18} The small residual uncertainty results mainly from the error bar determined by the fitting procedure described in the following and is strongly correlated to the signal-to-noise (S/N) ratio. We also note that the intensity of the absorption signal has been improved by two orders of magnitude as compared to our previous pulsed-CRDS measurements that were performed under identical experimental conditions (same backing pressure, same carrier gas, same sample temperature, and same applied voltage) with a cw slit jet expansion.⁹ The combination of various factors [such as a longer and wider slit, an improved mixing of the seed molecules (PAHs) with the carrier gas] has contributed to the enhancement of the absorption signal. Inversely, the lower reproducibility of the hydrodynamic conditions in pulsed expansion flows as opposed to cw conditions leads to about one order of magnitude increase of the level of noise in the signal. The result of these competing factors is a net S/N gain of a factor 10 in the present measurements.

The strongest absorption peak at 670.70 nm is assigned to the band origin. The band is broad, unresolved, with two weaker broad features at lower energy. Considering the maximum extent of the rotational structure—4 to 6 cm^{-1} —that is expected for a molecule the size of naphthalene for a rotational temperature of 20–100 K in the supersonic slit jet expansion²¹ and the absence of substructure, we conclude that unresolved rotational structure cannot account for the observed bandwidth. The broadening of the spectrum is characteristic of a nonradiative relaxation process of the excited state through internal conversion followed by intramolecular vibrational redistribution of the energy.^{18,22} In the statistical limit, it translates in the frequency domain into a homogeneous broadening characterized by a Lorentzian profile with a width that is proportional to the inverse of the time scale of the relaxation process. The fitting of the two stronger peaks leads to a full width at half maximum of $\Gamma = 25 \text{ cm}^{-1}$ for each band (see Table I). A lower limit of $1/2\pi\Gamma = 212$ fs is derived for the relaxation time in excellent agreement with the 200 fs value that was recently derived from a femtosecond transient grating spectroscopy study of the internal conversion of the naphthalene cation isolated in a

TABLE II. Absorption peak positions of the $D_2 \leftarrow D_0$ vibronic transitions of Np^+ and its associated vdW complexes with argon.

Assignment		Np^+		$\text{Np}^+ - \text{Ar} (1/0)$		$\text{Np}^+ - \text{Ar}_2 (1/1)$	
		λ (nm) ^a	ν (cm^{-1})	λ (nm)	ν (cm^{-1})	λ (nm)	ν (cm^{-1})
0	PDN-CRDS ^b	670.70	14905.7	672.53	14865	674.53	14821
	Photodepletion ^c		14906		14863		14820
$\nu_9(a_g)$	PDN-CRDS	648.89	15406.7	650.48	15369		
	Photodepletion		15408		15365		15322

^aAs intramolecular processes dominate the dynamics, the main absorption peaks of Np^+ and its vdW satellites (1/0) and (1/1) are expected to exhibit the same Lorentzian profile. The bands are fitted accordingly and lead to $\Delta\nu = 25 \text{ cm}^{-1}$.

^bThis work.

^cPino *et al.* (Ref. 18).

solid matrix.²³ Furthermore, the bandwidths measured here are similar to the intrinsic bandwidths observed by photodissociation of the $\text{Np}^+ - \text{Ar}$ van der Waals complex¹⁸ clearly indicating that the discharge *does not* significantly affect the vibrational temperature of the aromatic ions in the cold plasma expansion. As the lifetimes associated with the cooling process of the PAH ions (mainly by IR cascade emission on a millisecond time scale) greatly exceed the residence time of the Ar atoms in the active region of the plasma ($\tau_{\text{res}} \sim 3 \mu\text{s}$), these observations seem to indicate that the aromatic molecules are *softly* ionized (i.e., that the ions conserve the vibrational state of their neutral precursors). Ion production mechanisms are discussed in detail in Sec. III C. Finally, we note that the bandwidths measured in the cw-jet CRDS experiments were up to 1.5 times larger than the values measured in the current work (see Table I). These differences may be partly explained by the lower S/N in the earlier results even if other effects due to different plasma conditions (e.g., probing between the electrodes) cannot be completely ruled out.

The weak band seen at 672.53 nm (14865 cm^{-1}) in the spectrum (see Fig. 4) is assigned to the vibrationless electronic transition of the (1/0) $\text{Np}^+ - \text{Ar}$ van der Waals (vdW) complex that is also formed in the expansion. We measure a value of -41 cm^{-1} for the vdW shift induced by one argon atom in excellent agreement with the value of -43 cm^{-1} that has been reported for the electronic transition $D_2 \leftarrow D_0$.¹⁸ The spectral signature of the $\text{Np}^+ - \text{Ar}$ vdW (1/0) complex is also weakly detected at 38 cm^{-1} to the red of the second band absorption at 648.89 nm ($D_2(\nu_9) \leftarrow D_0$). Weaker signal intensities have precluded the detection of the spectral signature of the vdW complex associated with the 612.52 ($D_2(\nu_4) \leftarrow D_0$) and 593.35 nm ($D_2(\nu_9 + \nu_4) \leftarrow D_0$) bands. It has also been shown²⁴ that the vdW shift doubles when a second inert gas atom binds in an adsorption site of the aromatic unit that is equivalent to the one occupied by the first atom. This so-called shift additivity rule is also valid for ionic vdW complexes since little geometric change is expected after ionization of large molecular species. Vibrational analysis of matrix-isolated spectra also indicate that there is no significant deformation of the molecular skeleton

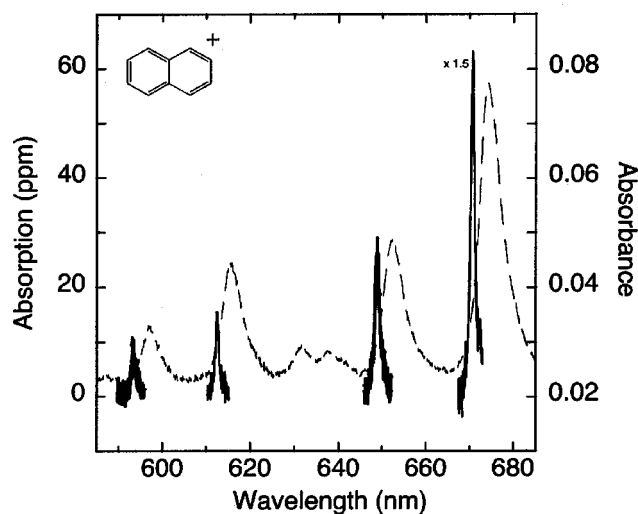


FIG. 5. Comparison of cavity ringdown spectroscopy (CRDS)—solid line—and Ne matrix isolation spectroscopy (MIS)—dashed line—measurements of the vibronic progression of the $D_2 \leftarrow D_0$ electronic transition band system of Np^+ . Since the vibronic bands were all measured individually in separate spectral windows, relative intensities are scaled using the data available in the literature (Ref. 9 and 18) (see the text for more details).

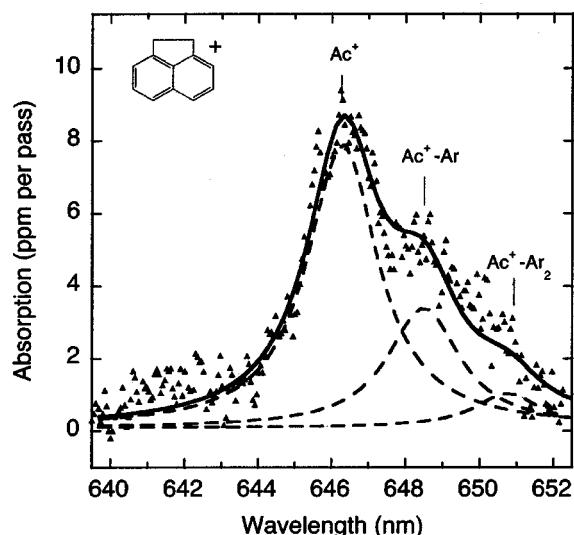


FIG. 6. The origin band of the $D_2 \leftarrow D_0$ electronic absorption band system of the cold acenaphthene ion in the gas phase measured by CRDS. The small dashed traces correspond to the three components which are required to reproduce the measured band profile (solid line).

TABLE III. Absorption peak positions corresponding to the $D_2 \leftarrow D_0$ vibrationless electronic transition of Ac^+ and its associated vdW complexes with argon.

	Ac^+		$\text{Ac}^+ - \text{Ar} (1/0)$		$\text{Ac}^+ - \text{Ar}_2 (1/1)$	
	λ (nm) ^a	ν (cm^{-1})	λ (nm)	ν (cm^{-1})	λ (nm)	ν (cm^{-1})
PDN-CRDS ^b	646.27	15469.1	648.6	15418	650.8	15367
Photodepletion ^c	646.23 ± 0.3	15470	648.5 ± 0.3	15416	650.7 ± 0.3	15364

^aAs intramolecular processes dominate the dynamics, the main absorption peaks of Ac^+ and its two vdW satellites (1/0) and (1/1) are expected to exhibit the same Lorentzian profile and are fitted accordingly and lead to $\Delta\nu = 55 \text{ cm}^{-1}$.

^bThis work.

^cBréchnignac *et al.*, private communication (Ref. 30).

of PAHs upon ionization (see e.g., Refs. 19 and 25). Taking advantage of the high quality S/N associated with the strongest Np^+ vibrationless transition band and relying on the shift additivity rule, we assign the peak located at 14821 cm^{-1} (-44 cm^{-1} from $\text{Np}^+ - \text{Ar}$) to the $\text{Np}^+ - \text{Ar}_2$ (1/1) complex (i.e., a vdW complex with an argon atom on each side of the plane of the carbon skeleton). Figure 4 shows that the bare Np^+ ion and the $\text{Np}^+ - \text{Ar}$ (1/0) and $\text{Np}^+ - \text{Ar}_2$ (1/1) vdW complex absorption bands exhibit very similar broadenings. As intramolecular processes dominate the dynamics, the excited Np^+ and its complexes with argon will follow the same relaxation pathways.¹⁸ This implies that Np^+ and its vdW satellites (1/0) and (1/1) will exhibit the same Lorentzian profile. The bands are fitted accordingly leading to the bandwidth reported in Table II. The bare Np^+ ion absorption band and the (1/0) and (1/1) vdW argon complex satellite bands exhibit an intensity ratio of 20:6:1 (see Fig. 4).

The absorption spectra of Np^+ measured in the gas (solid line) and solid phases (dotted line) are compared in Fig. 5. The dotted line represents the absorption spectrum of Np^+ trapped and isolated in a Ne cryogenic matrix maintained at a temperature of 5 K.¹⁹ Although the two spectra are similar, this comparison clearly illustrates the need for gas-phase data to unambiguously identify the carriers of the diffuse interstellar bands or any free interstellar molecular species for that matter (see Sec. I). Two major effects induced by the solid phase environment are observed in the spectrum of the matrix-isolated Np^+ . First, a redshift in energy in the band positions of the MIS measurements compared to the gas-phase data. In this specific case, we measure a band shift in energy of about 0.5% to the red (or 75 cm^{-1}) when Np^+ is trapped into a neon matrix (see Table I) in agreement with previous gas-phase studies.^{9,18} In addition to a significant shift in energy, the interactions between the host lattice and the trapped molecular ion induce a broadening of the bands (of the order of four to five times the intrinsic bandwidth as evidenced in Fig. 5).

B. The acenaphthene ion ($\text{C}_{12}\text{H}_{10}^+$)

Acenaphthene belongs to the chemical class of hydrogenated PAHs (i.e., PAHs with an excess of hydrogen). Acenaphthene has been found in meteorites along with numerous regular PAHs.²⁶ Recent laboratory studies of the photostability of a variety of PAHs show that the presence of sp^3

hybridized C atoms increases the propensity for H-loss.²⁷ Because of the reduced stability of hydrogenated PAHs compared to regular PAHs, the acenaphthene molecule is a good candidate to test the conditions in which the aromatic ions are formed in the cold plasma expansion (i.e., if they are indeed formed by soft Penning ionization).

The direct absorption spectrum of the acenaphthene ion (Ac^+) in the gas phase is reported for the first time. Acenaphthene is a planar hydrocarbon that belongs to the C_{2v} symmetry group. We follow the choice of long (x) and short (y) axes adopted for naphthalene. The electronic states involved in the transition are assigned based on recent MIS results.²⁰ In this paper, we report the vibrationless $B_2(D_2) \leftarrow XA_2(D_0)$ electronic absorption spectrum of Ac^+ , peaking at 646.3 nm. Figure 6 shows the spectrum measured at a reservoir temperature of 90°C (sample vapor pressure of 0.528 Torr^{28}), under 760 Torr backing pressure of argon and an applied voltage of -500 V . The intensity of the absorption signal of Ac^+ is six times weaker than for Np^+ , consistent with the fact that acenaphthene has a vapor pressure that is five times lower than that of naphthalene while the transitions associated with the two cations have comparable oscillator strengths (of the order of 0.1) as measured by MIS²⁰ and predicted by theoretical calculations.²⁹ Bréchnignac and co-workers have also recently studied this cation by the laser photodepletion technique in a molecular beam³⁰ and their experimental values are given for comparison in Table III. The band measured by PDN-CRDS exhibits a strong asymmetry in its profile that we assign to the contribution of the $\text{Ac}^+ - \text{Ar}$ (1/0) and $\text{Ac}^+ - \text{Ar}_2$ (1/1) vdW complexes. Following the described above procedure, the band profile has been fit with the sum of three Lorentzians with the same width and equally spaced. This fitting procedure results in a bandwidth of 2.3 nm (55 cm^{-1}) corresponding to a relaxation time of 100 fs. The bandwidth is twice as broad as that of the naphthalene ion. The position of the main peak at 646.27 nm is very close to the value of $646.2 \pm 0.3 \text{ nm}$ derived from Ref. 30. The $\text{Ac}^+ - \text{Ar}$ (1/0) and $\text{Ac}^+ - \text{Ar}_2$ (1/1) vdW complexes absorption bands peak at 648.6 and 650.8 nm, respectively, and are shifted to the red by 52 and 104 cm^{-1} , respectively. The peak positions of the (1/0) and (1/1) complexes are consistent with the values obtained in Ref. 30. One should, however, note that the uncertainty on the determination of the peak positions of the (1/0) and (1/1) complexes depends strongly on the peak intensity in the case of broad spectral

features, and is as high as ± 0.2 and ± 0.4 nm, respectively. Table III summarizes the results. The electronic absorption band of the Ac^+ molecular ion is redshifted by 0.3% (or 42 cm^{-1}) when it is trapped in a neon matrix (648.1 nm) and its width is about 3.9 nm (92 cm^{-1}) or 1.7 times its value in the gas phase.²⁰ The value of the frequency shift when going from the gas phase to the solid phase is lower here than in the case of Np^+ . This effect might be due to the increased rigidity of the molecular skeleton of acenaphthene by the presence of three additional C–C bonds as compared to naphthalene. This increased rigidity would tend to minimize the perturbation (deformation) induced on the molecular structure by the solid lattice of the neon matrix. Finally we note that, in this case, the intensity ratio of the bare ion (Ac^+) with its (1/0) and (1/1) complexes is 7.5:3.0:1.0.

C. Production mechanism of the aromatic ions

This section addresses the formation mechanisms of the aromatic ions in the discharge. This is an essential step toward modeling the physical conditions in the plasma (vibrational temperature, density) and optimization of the ion source. It is also a key requirement, in our specific case, to assess the relevance of this experimental approach to simulate interstellar conditions (free, cold ions). The following discussion will focus on the naphthalene ion because it is the polycyclic aromatic ion that has been the most extensively studied in the gas phase. The conclusions are, however, general for this class of aromatic ions.

Based on the CRDS measurement of an absolute absorption of 50 ppm per pass for the strongest band of Np^+ at 670.70 nm and on the determination by R2P2CI of an absorption cross section of $4.6 \times 10^{-16} \text{ cm}^2$ for this same band,¹⁸ the molecular ion density is estimated to be 10^{10} cm^{-3} in the probed postdischarge region 2 mm downstream from the sharp jaws (i.e., 3.5 mm from the origin of the planar expansion). This value translates into a 10^{-5} ionization efficiency when taking into account the dilution factor of neutral naphthalene in Ar of 0.3% at a backing pressure of Ar of 800 torr ($p_{\text{Np}} = 2.6 \text{ Torr}$ at 66°C) and when adopting the neutral aromatic molecular density derived from the hydrodynamics equations in the case of a planar expansion generated with a 200- μm -wide, 10-cm-long slit ($n_{\text{Np}} = 10^{15} \text{ cm}^{-3}$ at 3.5 mm from the origin of the planar expansion).³¹

As a consequence of supersonic velocities ($5 \times 10^4 \text{ cm/s}$ for Ar atoms), the ion precursors spend 3 μs in the discharge environment. During this short residence time, Ar atoms and aromatic molecules are bombarded by $(i/q)/A \times \tau_{\text{res}} = 5 \times 10^{12} \text{ electrons/cm}^2$ where $A \sim 20 \text{ mm}^2$ is the plasma cross section and $i \sim 50 \text{ mA}$ is the current.

The aromatic ions can be generated in the discharge from their neutral precursors through three channels of formation.

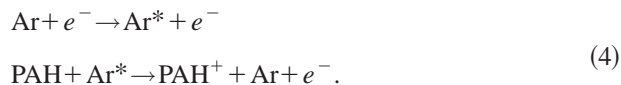
(i) By electron impact (EI) with energies higher than the ionization potential (IP) of the neutral precursor (IP range between 6 and 8.5 eV for PAHs),



(ii) By charge transfer (CT) between neutral PAH precursors and ionized carrier gas atoms,



or (iii) through Penning ionization (PI) of the neutral precursors by metastable argon atoms,



Penning ionization appears to be the dominant channel for the formation of cold PAH ions in the discharge as we discuss in the following.

Mass spectrometry studies show that the outcome of the collision of an electron with an aromatic target depends strongly on the energy of the projectile. For example, at the standard high-energy mode of most mass spectrometers (i.e., at electron energy of about 70 eV), the most probable outcome of the collision is the fragmentation of the molecule. In the case of naphthalene, two-thirds of the molecules ionized end up fragmented³² while one-third are ionized in various electronic excited states. Photoion mass spectrometry studies have identified the loss of $-\text{H}$, $-\text{C}_2\text{H}_2$, and $-\text{H}_2$ as the primary fragmentation channels.³³ A significant fraction of the remaining naphthalene ions, formed in their D_n excited electronic states, undergo rapid intramolecular vibrational relaxation (IVR) on a picosecond time scale followed by internal conversion (IC) to lower electronic states with the same spin multiplicity until they reach their ground electronic state D_0 with a high vibrational energy. Fluorescence transitions are not expected to play a major role given their estimated low quantum yield and the molecular ions cool primarily through infrared emission with a millisecond time scale.³⁴ The time scale of the radiative cascade emission is thus orders of magnitude larger than the time of flight of the molecular ions to the probed postdischarge region ($\sim 4.5 \mu\text{s}$). One of the effects of EI in our experiment is therefore to reduce dramatically the population of aromatic ions formed in their ground state. It is difficult to quantify the depletion of the vibrational ground state at this point because the naphthalene EI ionization cross section and the mean electron energy in the plasma are unknown. The latter is difficult to model because of the strong density gradient in the supersonic jet and the particular geometry of the discharge arrangement. Thus, we estimate that EI is a minor channel for the formation of cold molecular Np^+ ions.

The hypothesis of a very limited contribution of EI is supported by the observation of the collapse of the aromatic ion signal when a small fraction (a few percent) of neon or helium is introduced in the carrier gas. If EI is a major production channel, the ion yield should be independent of a slight change in the composition of the carrier gas mixture. Also the observation of a change in the glow color from blue/violet to orange/red when Ne is added to the carrier gas or to white/green when He is added indicates that a significant fraction of Ne/He atoms are excited or ionized. This means, in other words, that electrons with energies higher than 19.82 eV (3S_1 He*, first metastable state) are produced

in the chamber. These observations imply that the Ne/He metastable atoms *do not* efficiently transfer their energy to the neutral aromatics. In particular, they provide an upper energy limit of 16.62 eV (3P_2 Ne*, first metastable state) for efficient ionization of the aromatic molecules in the discharge.

These findings are corroborated by two recent experimental studies. The first study shows that organic molecules with an 8 eV ionization potential are heavily fragmented upon bombardment with metastable atom with energies higher than 16 eV (Ne* and He* metastable atoms).³⁵ The same conclusions are reached by selected ion flow tube studies of the branching ratio and the rate constants for the reaction of a variety of positive ions with naphthalene at high temperature.³⁶ They determined a 16 eV dissociation threshold for the naphthalene cation, a value substantially higher than the H loss threshold (15.41 eV appearance energy²⁷) because of kinetic shifts and quenching by collisions with the helium buffer gas.³⁶ Because of the collisionless environment provided by a supersonic expansion, the fragmentation threshold should be lower in our experiment. As the ionization potential of Ar lies just above the fragmentation threshold at 15.75 eV ($^2P_{1/2}$ and $^2P_{3/2}$ states), it nevertheless means that the charge transfer of Ar⁺ to the neutral Np is not an efficient process and leads in most of the cases to the heating and the fragmentation of the target aromatic molecule. Thus, we estimate that CT is also a minor channel for the formation of *cold* molecular Np⁺ ions and conclude that the dominant process of ion formation in the plasma is through Penning ionization (PI) of the neutral precursors with metastable argon atoms (11.55 eV 3P_2 active metastable state).

In PI, the electronically excited metastable atoms have diffuse outer orbitals, giving rise to relatively soft intermolecular repulsion in nonbonded excited state potentials. A low energy ionizing collision is then *near* adiabatic in respect to its effect on the vibrations of the target molecule (i.e., the wave functions and Franck–Condon factors are undisturbed by the ionizing collision).³⁷ The final vibrational states produced by Penning ionization will thus depend on the Franck–Condon overlap of the vibrational wave functions of the initial state (electronic ground state of the neutral aromatic precursor, S_0) with the final state (electronic state of the aromatic ion).³⁸ The photoelectron spectra of Np³⁹ show that the $D_0 \leftarrow S_0$ transition is effectively a near vertical ionization process confirming that the aromatic ions are formed through a soft ionization mechanism in our source. The fragmentation of the aromatic molecules upon EI and CT may explain the observed deposit of soot on the electrodes. It is expected that the ionization yield increases as a reciprocal function of the energy gap between the ionization potential (IP) of the target molecule and the energy of the metastable carrier gas atom. Heavier carrier gas—such as Krypton (Kr* 3P_2 , 9.92 eV, active metastable state)—might be required to ionize larger PAHs (with lower IPs).

IV. CONCLUSION

The absorption spectra of cold, free, naphthalene ($C_{10}H_8^+$) and acenaphthene ($C_{12}H_{10}^+$) cations formed in a free

jet planar expansion are reported and discussed. Two vibronic bands associated with the $^2B_{3g}(D_2) \leftarrow X^2A_u(D_0)$ electronic band system of the cold naphthalene cation ($C_{10}H_8^+$) and the vibrationless $B_2(D_2) \leftarrow XA_2(D_0)$ electronic transition of the cold acenaphthene cation ($C_{12}H_{10}^+$) are reported for the first time through direct absorption measurements in the gas phase. Direct absorption spectra of vdW complexes of the type PAH⁺–Ar (1/0) and PAH⁺–Ar₂ (1/1) are also reported. The spectral characteristics of the bands are discussed and analyzed in view of the limited data available for PAH ions in the gas phase (CRDS cw slit-jet experiment⁹ and R2P2CI molecular depletion data^{18,30,40}). The characteristics of the pulsed discharge nozzle–cavity ringdown spectrometer (PDN-CRDS) system developed in our laboratory to measure the spectra of interstellar aromatic analogs under conditions that are relevant to astrophysics are discussed. An attempt is also made to identify the main formation mechanism(s) of the aromatic ions in the discharge.

The main conclusions that are derived from this study are the following.

(1) The PAH ions that are generated in the plasma of the PDN source are primarily formed through soft PI of the neutral precursor minimizing vibrational heating.

(2) As a result, the PAH ions that are formed in the expansion are cold (vibrational temperature of the order of 100–150 K) leading to the measurement of the *intrinsic profiles* of the spectral (vibronic) bands.

(3) The bandwidths of the vibronic bands of free PAH ions are intrinsically broad due to femtosecond, nonradiative, intramolecular relaxation mechanisms (IC combined with IVR) that mask the rotational structure as can be derived by comparison with the R2P2CI molecular depletion findings.

(4) The ionization yield is low (of the order of 10^{-5}) due to the competition of the PI channel with the fragmentation channels of the neutral PAH precursor through EI and CT.

(5) Penning ionization makes the ionization yield strongly dependent upon the nature of the carrier gas.

(6) vdW clusters of the type PAH⁺–Ar (1/0) and PAH⁺–Ar₂ (1/1) are formed and observed in the jet expansion. The measured vdW shifts associated with these clusters verify the additivity rule.

(7) Comparison of the gas-phase spectra with matrix-isolation spectroscopy data permits quantification of the perturbations induced by solid inert gas matrices in the case of the naphthalene and acenaphthene molecular cations. Redshifts of 0.5% and 0.3% are found in the band peak positions of the naphthalene⁺ and the acenaphthene⁺ ions, respectively, when isolated in solid neon. The solid neon matrix also induces band broadening of the order of two to five times the intrinsic bandwidth.

In conclusion, a PDN-CRDS system has been developed to measure the direct absorption spectra of large (i.e., more than 10 carbon atoms) aromatic ions in a free jet planar expansion. This information is essential for astrophysical studies because it allows one to *directly* compare laboratory spectra with astronomical observations of the interstellar medium in the UV-NIR range (e.g., Hubble Space Telescope). It also expands the frontiers of molecular spectroscopy and dynamics into the—for the most part—unexplored domain of large

molecular ions. We have focused here on the analysis of the experimental results and on the discussion of the characteristics of the experimental system. The astrophysical implications will be treated in an upcoming article.

ACKNOWLEDGMENTS

This work is supported by the NASA SARA Program (RTOP No. 188-01-00-21). J.J.S. acknowledges support from the NASA SBIR Project No. NAS2-99045. L.B. is a National Research Council Associate at NASA-Ames Research Center. The authors wish to acknowledge R. Walker for outstanding technical support. The authors are also grateful to A. O'Keefe for the invaluable support he has provided to this project and to R. Saykally for providing the design of the PDN source. We are grateful to Ph. Bréchnignac for providing data prior to publication. Useful discussions with D. Romanini are also acknowledged.

- ¹F. Salama, in *Solid Interstellar Matter: The ISO Revolution* (EDP Sciences, France, 1999), pp. 65–87.
- ²K. Sellgren, *Spectrochim. Acta, Part A* **57**, 627 (2001).
- ³L. J. Allamandola, A. G. G. M. Tielens, and J. R. Barker, *Astrophys. J. Lett.* **290**, L25 (1985).
- ⁴A. Léger and L. B. d'Hendecourt, *Astron. Astrophys.* **146**, 81 (1985).
- ⁵G. H. Herbig, *Annu. Rev. Astron. Astrophys.* **33**, 19 (1995).
- ⁶*The Diffuse Interstellar Bands*, edited by A. G. G. M. Tielens and T. P. Snow (Kluwer Academic, Dordrecht, 1995).
- ⁷T. Henning and F. Salama, *Science* **282**, 2204 (1998).
- ⁸F. Salama, E. Bakes, L. J. Allamandola, and A. G. G. M. Tielens, *Astrophys. J.* **458**, 621 (1996).
- ⁹D. Romanini, L. Biennier, F. Salama, A. Kachanov, L. J. Allamandola, and F. Stoeckel, *Chem. Phys. Lett.* **303**, 165 (1999).
- ¹⁰P. Bréchnignac and T. Pino, *Astron. Astrophys.* **343**, 49 (1999).
- ¹¹S. Davis, D. T. Anderson, G. Duxbury, and D. J. Nesbitt, *J. Chem. Phys.* **107**, 5661 (1997).
- ¹²K. Liu, R. S. Fellers, M. R. Viant, R. P. McLaughlin, M. Brown, and R. Saykally, *Rev. Sci. Instrum.* **67**, 410 (1996).
- ¹³D. R. Wagner (private communication).
- ¹⁴A. O'Keefe and D. A. G. Deacon, *Rev. Sci. Instrum.* **59**, 2544 (1988).
- ¹⁵A. Savitzky and M. J. E. Golay, *Anal. Chem.* **36**, 1627 (1964).
- ¹⁶W. C. Martin, J. R. Fuhr, D. E. Kelleher, A. Musgrove, L. Podobedova, J. Reader, E. B. Saloman, C. J. Sansonetti, W. L. Wiese, P. J. Mohr, and K. Olsen, NIST Atomic Spectra Database (version 2.0). Available: <http://physics.nist.gov/asd>. (National Institute of Standards and Technology, Gaithersburg, MD, 2002).
- ¹⁷T. Motylewski and H. Linnartz, *Rev. Sci. Instrum.* **70**, 1305 (1999).
- ¹⁸T. Pino, N. Boudin, and P. Bréchnignac, *J. Chem. Phys.* **111**, 7337 (1999).
- ¹⁹F. Salama and L. J. Allamandola, *J. Chem. Phys.* **94**, 6964 (1991).
- ²⁰T. Halasinski and F. Salama (unpublished).
- ²¹C. Cossart-Magos and S. Leach, *Astron. Astrophys.* **233**, 559 (1990).
- ²²R. Englman and J. Jortner, *Mol. Phys.* **18**, 145 (1970).
- ²³R. A. Crowell, E. L. Chronister, R. Lian, A. D. Liu, S. Pommeret, I. A. Shkrob, A. D. Trifunac, and L. Zhao, (2002), *J. Phys. Chem. A* (to be published).
- ²⁴P. Hermine, P. Parneix, B. Coutant, F. G. Amar, and P. Bréchnignac, *Z. Phys. D: At., Mol. Clusters* **22**, 529 (1992).
- ²⁵F. Salama, C. Joblin, and L. J. Allamandola, *J. Chem. Phys.* **101**, 10252 (1994).
- ²⁶A. Shimoyama, *Adv. Space Res.* **19**, 1045 (1997).
- ²⁷H. W. Jochims, H. Baumgärtel, and S. Leach, *Astrophys. J.* **512**, 500 (1999).
- ²⁸K. Nass, D. Lenoir, and A. Kettrup, *Angew. Chem. Int. Ed. Engl.* **34**, 1735 (1995).
- ²⁹T. Bally, C. Carra, M. P. Fülcher, and Z. Zhu, *J. Chem. Soc., Perkin Trans. 2* **1998**, 1759.
- ³⁰P. Bréchnignac (private communication).
- ³¹*Atomic and Molecular Beam Methods*, edited by G. Scoles (Oxford University Press, New York, 1988).
- ³²*IR and Mass Spectra*, in NIST Chemistry WebBook, NIST Standard Reference Database Vol. 69, edited by P. J. Linstrom and W. G. Mallard. Available: <http://webbook.nist.gov> (National Institute of Standards and Technology, Gaithersburg, MD, 2001).
- ³³H. W. Jochims, E. Rühl, H. Baumgärtel, S. Tobita, and S. Leach, *Astrophys. J.* **420**, 307 (1994).
- ³⁴P. Boissel, P. de Parseval, P. Marty, and G. Lefèvre, *J. Chem. Phys.* **106**, 4973 (1997).
- ³⁵M. J. Bertrand, D. Faubert, S. Letarte, and M. Mousselmal (unpublished).
- ³⁶A. J. Midey, S. Williams, S. T. Arnold, I. Dotan, R. A. Morris, and A. A. Viggiano, *Int. J. Mass. Spectrom.* **195**, 327 (2000).
- ³⁷H. M. Bevsek and P. E. Siska, *J. Chem. Phys.* **102**, 1934 (1995).
- ³⁸P. E. Siska, *Rev. Mod. Phys.* **65**, 337 (1993).
- ³⁹P. A. Clark, F. Brogli, and E. Heilbronner, *Helv. Chim. Acta* **55**, 1415 (1972).
- ⁴⁰P. Bréchnignac, T. Pino, and N. Boudin, *Spectrochim. Acta, Part A* **57**, 745 (2001).